研究者による解析が困難になる。生体画像に特化したソフトウェアをデザイン・開発し、生体内の細胞を追跡・評価した。評価に際しては、標準化可能で定量性を持つことを優先した。パラメーターを観察者が調節するのではなく、ロバスト性をもってほぼ全自動で解析が終了するシステムを目指した。

(2) 解析ソフトウェアの開発

大型動物は特有の体動があり、実際上の画像取得を困難にしている。我々は生体のXYZT 画像に対し、体動をキャンセルし、従来のViewerで見えづらかった構造物を画像処理により明確にするソフトウェアを開発した。さらに、パターン認識を取り入れることで、XYZTイメージのなかにある細胞種を特異的に同定した。本技術により、ブタ体内にどのような細胞が分布し、どのように動いているかを三次元的にリアルタイムで捉えられる。

(3) 倫理面への配慮

本研究では動物実験が含まれる。動物愛護には最大限の配慮を払った。動物実験プロトコールは機関内承認を得た(自治医科大学 H26 年 4 月 18 日承認番号 14227 号)。

C. 研究結果

(1) ブタ用イメージングデバイスの開発

ブタの体内組織・細胞の詳細な可視化を目的として、一光子イメージングから二光子イメージングにシフトした。大型動物は臓器漿膜が厚く、深部イメージングが欠かせないこと、Z軸の解像度が必要なこと、が理由としてあげられる。技術的には困難であり、動物へのアクセスも難しいため、麻酔・外科処置をはじめとする全身管理の習熟を必要とした。

その結果、**図3**のような高解像度イメージングを達成した。ビデオレート(秒30コマ)の高速画像取得により、血流など動的変化を捉えることも可能である。

図4　腸管血管で同定したブタ血球(二光子生体イメージング)

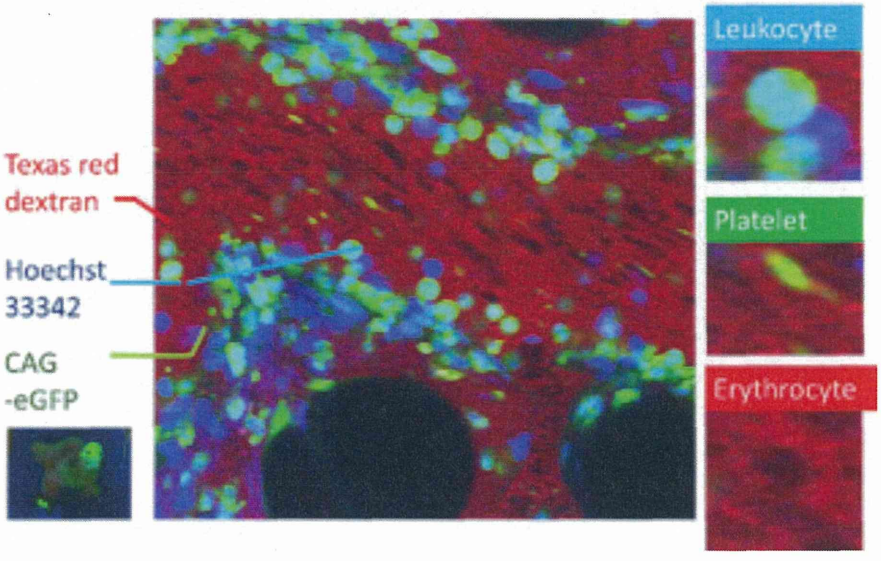

図5　生体イメージング用ソフトウェアの開発

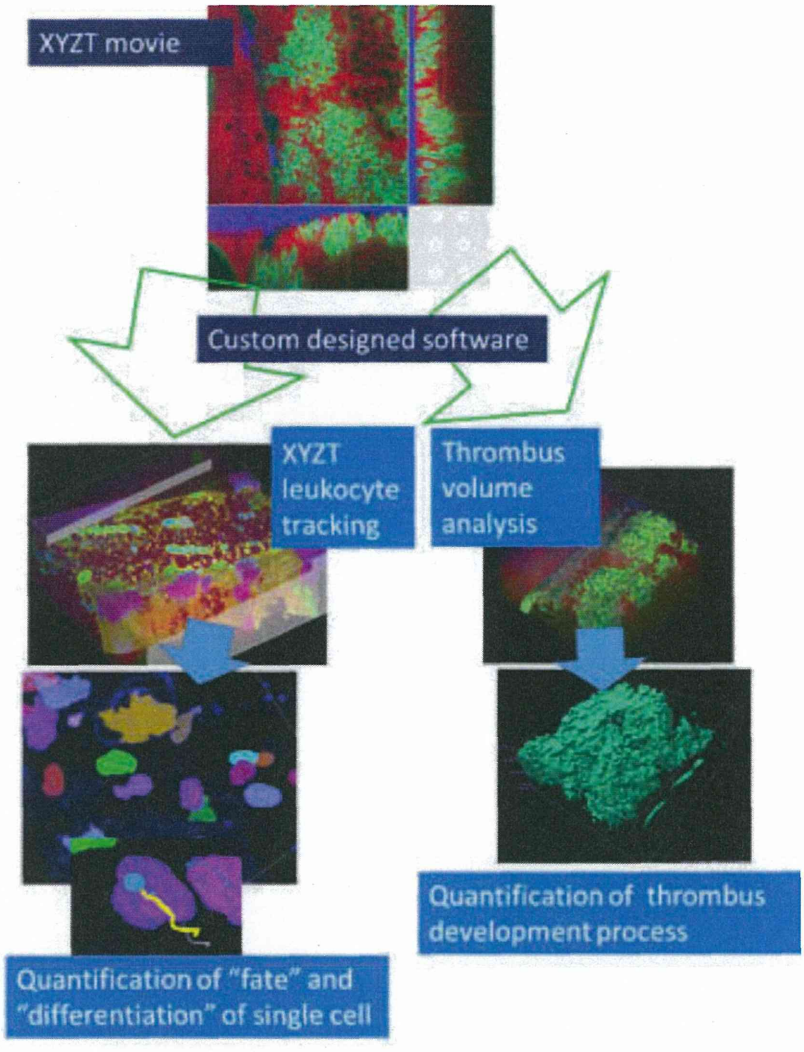

図6　生体イメージングで確認したヒト血小板のブタ以内動態

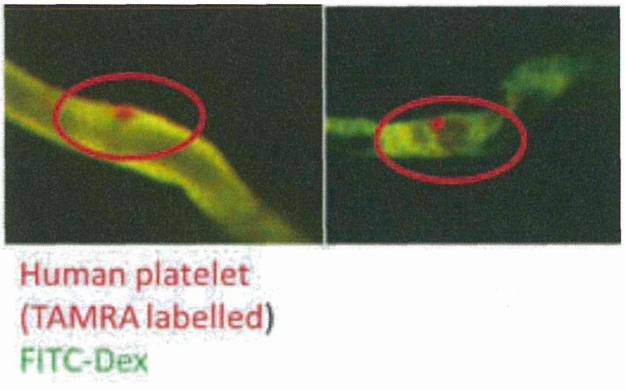

(2) 生体光分子イメージング法の開発

平成 26 年度にはマウスに加えて、実際にブタを用いた生体光分子イメージング法を行った。その際、遺伝子改変ブタ、Kusabira Orange, CAG-eGFP 発現ブタを用いた、二光子イメージングにより良好な画像を得ており(**図 4**)、一細胞、さらには、一血小板を同定している。

さらに、生体画像に特化したソフトウェアを開発し、白血球の追跡および血小板体積の定量的評価を可能にした。生体画像は多次元かつ大容量のため評価が困難である。今回開発したソフトウェアにより標準化を伴った数値化が可能になり、ブタイメージングを用いた創薬等のプロセスの裏付けになると考えられた。

今までマウスではレーザー傷害および活性酸素による血栓形成モデルを確立し、血栓形成過程の詳細を明らかにしている。特に、ヒト iPS 細胞由来人工血小板を TAMRA 染色で染め、NOG マウス内部で血栓形成を観察し、人工血小板が生体内で有効に働くことを確認している。今回、本システムを用いブタにおけるヒト末梢血血小板の動態を明らかにしており、今後、ヒト iPS 細胞由来血小板の解析を行う予定である。

D. 考察

本研究で開発する生体光分子イメージングは、ブタのみならずヒト臨床に応用出来る可能性が高い。本研究計画では今までの実績を生かして、光イメージングをマウスからブタに応用し、さらに、今まで不可能と考えられた大型動物における二光子イメージングを実現した。ブタにおいては一光子イメージングの適応は限定的であり、血管内部の血球動態を捉えるためには二光子顕微鏡を用いる必要がある。

さらに二光子イメージングでは非常に広範な臓器で画像取得が可能であった。たとえば、眼球、舌、といった実質臓器でも、深部構造を明瞭に可視化している(**図7**)。舌では

図7　生体イメージングによるブタ・マウスの舌および眼球画像

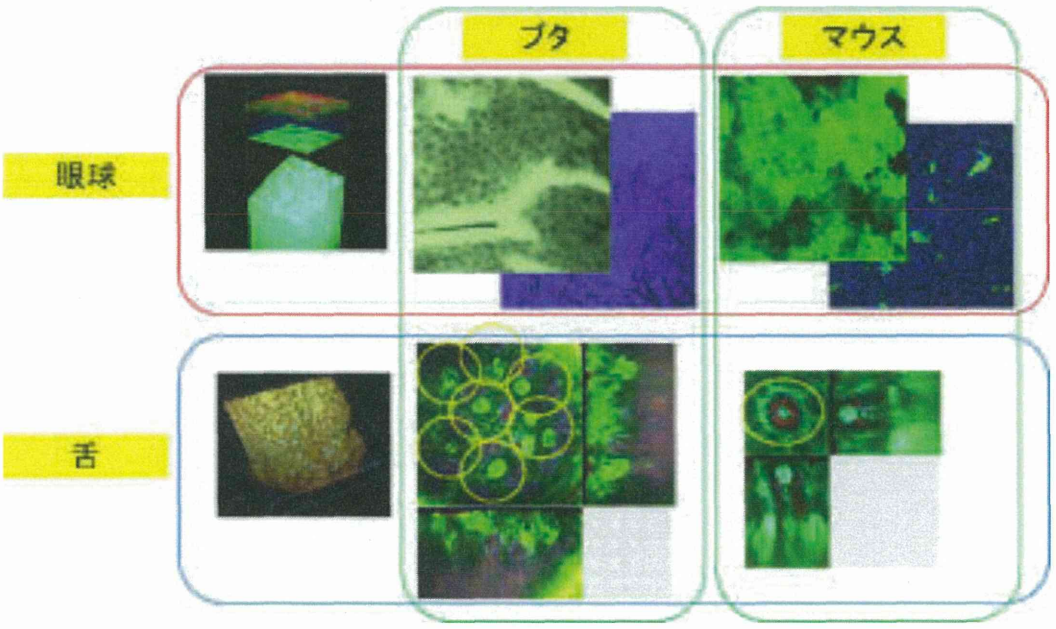

味知覚器官（黄色で図示）の組織構築がマウスとは異なり集塊を構成していることを確認している。将来的にヒトにおける光診断につながる知見と考えられた。

この、生体親和性の高い光イメージングにより、血液細胞、たとえば血小板の可視化が可能になり、ヒト血小板のブタにおける評価が可能になった。人工血小板の機能評価、抗血小板薬の薬効評価、など多くのアプリケーションが期待できる。さらに、心血管イベント発症の予測・リスク層別化・治療効果の予測と決定によるテイラーメイド医療に役立つと考えられる。イメージングの対象とは血管内の血球にとどまらず、骨髄中の造血幹細胞や、炎症部位のリンパ球・好中球など多岐にわたり、病態解明をめざした基礎研究のみならず、臨床応用への橋渡し・トランスレーションが可能になる。

E. 結論

平成 26 年度には実際にブタ生体内の血管を流れる赤血球、白血球、血小板を単一細胞レベルで可視化し、血栓形成過程を観察することに成功した。

F. 健康危険情報

（分担研究報告書には記入せずに、総括研究報告書にまとめて記入した。）

G. 研究発表

論文発表

1. Nishimura S, Nagasaki M, Kunishima S, Sawaguchi A, Sakata A, Sakaguchi H, Ohmori T, Manabe I, J Italiano, Ryu T, Takayama N, Komuro I, Kadowaki T, Eto K, Nagai R. Tentative title : IL-1α induces thrombopoiesis through megakaryocyte rupture in response to acute platelet needs *J Cell Biology* 2015 in publication
2. Nakamura, S., Takayama, N., Hirata, S., Seo, H., Endo, H., Ochi, K., Fujita, K.-I., Koike, T., Harimoto, K.-I., Dohda, T., Watanabe, A., Okita, K., Takahashi, N., Sawaguchi, A., Yamanaka, S., Nakauchi, H., Nishimura, S., Eto, K.: Expandable megakaryocyte cell lines enable clinically applicable generation of platelets from human induced pluripotent stem cells. *Cell Stem Cell* 2014 Apr. 3; 14(4): 535-548.(doi: 10.1016/j.stem.2014.01.011.) Epub 2014 Feb. 13.
3. Nishimura, S., Nagasaki, M., Okudaira, S., Aoki, J., Ohmori, T., Ohkawa, R., Nakamura, K., Igarashi, K., Yamashita, H., Eto, K., Uno, K., Hayashi, N., Kadowaki, T., Komuro, I., Yatomi, Y., and Nagai, R.: ENPP2 contributes to adipose Tissue expansion and insulin resistance in diet-induced obesity. *Diabetes* 2014; 63(12):4154–4164.
4. Tanaka, M., Ikeda, K., Suganami, T., Komiya, C., Ochi, K., Shirakawa, I., Hamaguchi, M., Nishimura, S., Manabe, I., Matsuda, T., Kimura, K., Inoue, H., Inagaki, Y., Aoe, S., Yamasaki, S., and Ogawa, Y.:

Macrophage-inducible C-type lectin underlies obesity-induced adipose tissue fibrosis. ***Nat. Commumnications***. 2014; 5:4982.

5. Kunishima, S., **Nishimura, S.**, Suzuki, H., Imaizumi, M., Saito, H.: TUBB1 mutation disrupting microtubule assembly impairs proplatelet formation and results in congenital macrothrombocytopenia. ***Eur. J. Haematol.*** 2014 Apr.; 92(4): 276-282. (doi: 10.1111/ejh.12252.) Epub 2014 Jan. 11.
6. Sakata, A., Ohmori, T., **Nishimura, S.**, Suzuki, H., Madoiwa, S., Mimuro, J., Kario, K., Sakata, Y.: Paxillin is an intrinsic negative regulator of platelet activation in mice. ***Thrombosis Journal***. 2014 Jan. 2; 12(1): 1. (doi: 10.1186/1477-9560-12-1.)

学会発表

1. **Nishimura, S.**,: Two photon high-speed XYZT imaging identify novel rapid 'rupture'-type thrombopoiesis from bone marrow megakaryocyte.Cell-Cell interactions in diseased conditions revealed by three dimensional and intravital two photon microscope: From visualization to quantification. Focus on Microscopy 2015, Germany, March 3- April 1, 2015.
2. **西村智**:生体角膜イメージング. 角膜カンファランス 2015, 高知, 2015 年 2 月 11 日-13 日
3. **Nishimura, S.**: Fluorescence Imaging of Cardiovascular Systems.International Symposium on Multi-dimensional Fluorescence Live Imaging of Cellular Functions and Molecular Activities (MDFLI), Kyoto, 2015, January, 26-28.
4. **西村智**:非線形顕微鏡と定量化手法による仮説抽出:機能形態融合型イメージングを目指して. 第37回日本分子生物学会年会, 横浜, 2014 年 11 月 25 日-27 日.
5. **Nishimura, S.**, Eto, K., Nagai, R.,: Thrombus development processes dependent on endothelial injuries: Visualized by in vivo imaging. Two modes of thrombopoiesis: Dynamically regulated by TPO and lL-1alpha balances. 第 76 回日本血液学会学術集会, 大阪, 2014 年 10 月 31 日-11 月 2 日.
6. **西村智**:蛍光生体分子イメージングによる生活習慣病へのアプローチ～形態をこえた形態学を目指して～. 第 11 回自治医大国際シンポジウム, 栃木, 2014 年 10 月 30 日.
7. **西村智**:二光子顕微鏡を用いた血管・間質相互作用の可視化解析. In vivo イメージングフォーラム 2014, 東京, 2014 年 10 月 23 日.
8. **西村智**:蛍光で見る造血・血栓・炎症 第 36 回 埼玉先端血液懇話会, 埼玉, 2014 年 10 月 17 日.
9. **西村智**:非線形顕微鏡を用いた多面的生体評価システムの開発. 創薬薬理フォーラム 第 22 回シンポジウム, 東京, 2014 年 9 月 26 日.
10. **Nishimura, S.**: Thrombus Development Processes are Determined by Endothelial

Injuries: Examined by In vivo Multi-photon Molecular Imaging. Artery Cell Contraction Processes via ROS and NO Balance Visualized by In Vivo Multi-photon Imaging and Laser Injury Technique. World Molecular Imaging Congress 2014, Seoul, 2014, September,17 -20.

11. 西村智:生体二光子イメージングによるマウス角膜傷害・炎症・再生過程の可視化. 第50回日本眼光学学会総会, 石川, 2014年9月6日-7日.
12. Nishimura, S., Eto, K., Nagai, R.: Top Rated Abstract in Platelet Physiology: Morphological Distinction Unravels Mechanisms of Platelet Biogenesis from Bone Marrow Megakaryocytes, Thrombus Development Processes Dependent on EndothElial Injuries: Visualized by In Vivo Two Photon Imaging. 60th Annual Meeting of the Scientific and Standardization Committee of the ISTH 2014, USA, 2014 July.23-26.
13. Nishimura, S.: Seeing the single platelet behavior in in vitro and living animals.XIII European Symposium on Platelet and Granulocyte Immunobiology 2014 ,Germany, July 3-6, 2014.
14. 西村智:炎症・免疫と生活習慣病:光を用いた解析. 第2回糖尿病トランスレーショナルリサーチ研究会, 大阪, 2014年7月1日-3日.
15. 西村智:蛍光・燐光生体イメージングによる病態解析. 群馬大学理工学部大学院セミナー, 群馬, 2014年6月18日.
16. 西村智, 江藤浩之, 永井良三: サイトカインバランスにより規定される血小板造血モード:分子イメージングによる可視化解析、生体非線形イメージングを用いた血栓形成過程における内皮・血小板・白血球クロストークの解明 2014.5.29~31 平成26年5月29-31日第36回日本血栓止血学会学術集会, 大阪, 2014年5月29日-31日.
17. 西村智:生体二光子イメージングによる炎症病態解析 In vivo multi-photon imaging of inflammatory diseases. 第70回日本顕微鏡学会,千葉, 2014年5月10日-12日.
18. Nishimura, S. : Artery cell contraction via ROS and NO balance visualized by in vivo multi-photon imaging technique. Focus on Microscopy 2014, USA, April 13-16, 2014.

H. 知的財産権の出願・登録状況

特許

1. 西村智「血小板解析方法及び血小板解析システム」特願2010-125869 (H22年6月1日申請、平成26年9月12日許諾)

別紙4

研究成果の刊行に関する一覧表

書籍

著者氏名	論文タイトル名	書籍全体の編集者名	書　籍　名	出版社名	出版地	出版年	ページ
なし							

雑誌

発表者氏名	論文タイトル名	発表誌名	巻号	ページ	出版年
Nakamura, S., Takayama, N., Hirata, S., Seo, H., Endo, H., Ochi, K., Fujita, K.-I., Koike, T., Harimoto, K.-I., Dohda, T., Watanabe, A., Okita, K., Takahashi, N., Sawaguchi, A., Yamanaka, S., Nakauchi, H., **Nishimura, S.**, and Eto, K.	Expandable megakaryocyte cell lines enable clinically applicable generation of platelets from human induced pluripotent stem cells	Cell Stem Cell	vol. 14, no. 4	535–548	2014
Kunishima, S., **Nishimura, S.**, Suzuki, H., Imaizumi, M., and Saito, H.	TUBB1 mutation disrupting microtubule assembly impairs proplatelet formation and results in congenital macrothrombocytope-nia	European Journal of Haematology	vol. 92, no. 4	276–282	2014
Abe, T., **Hanazono, Y.**, and Nagao, Y.	A long-term follow-up study on the engraftment of human hematopoietic stem cells in sheep	Experimental Animals	vol. 63, no. 4	475–481	2014

発表者氏名	論文タイトル名	発表誌名	巻号	ページ	出版年
Mizukami, Y., Abe, T., Shibata, H., Makimura, Y., Fujishiro, S.H., Yanase, K., Hishikawa, S., Kobayashi, E., and **Hanazono, Y.**	MHC-matched induced pluripotent stem cells can attenuate cellular and humoral immune responses but are still susceptible to innate immunity	PLoS One	vol. 9, no. 6	e98319	2014
Matsunari, H., Kobayashi, T., Watanabe, M., Umeyama, K., Nakano, K., Kanai, T., Matsuda, T., Nagaya, M., Hara, M., Nakauchi, H., and **Nagashima, H.**	Transgenic pigs with pancreas specific expression of green fluorescent protein	The Journal of Reproduction and Development	vol. 60, no. 3	230–237	2014
Hoang, D.-T., Matsunari, H., Nagaya, M., **Nagashima, H.**, Millis, J.M., Witkowski, P., Periwal, V., Hara, M., and Jo, J.	A conserved rule for pancreatic islet rganization	PLoS One	vol. 9, no. 10	e110384	2014
Hara, S., Umeyama, K., Yokoo, T., **Nagashima, H.**, and Nagata, M.	Diffuse glomerular nodular lesions in diabetic pigs carrying a dominant- negative mutant hepatocyte nuclear factor 1-alpha, an inheritant diabetic gene in humans	PLoS One	vol. 9, no. 3	e92219	2014
Sekijima, M., Waki, S., Sahara, H., Tasaki, M., Wilkinson, R.A., Villani, V., Shimatsu, Y., Nakano, K., Matsunari, H., **Nagashima, H.**, Fishman, J.A., Shimizu, A., and Yamada, K.	Results of life-supporting galactosyltransferase knockout kidneys in cynomolgus monkeys using two different sources of galactosyltransferase knockout Swine	Trans-plantation	vol. 98	419–426	2014

発表者氏名	論文タイトル名	発表誌名	巻号	ページ	出版年
Miyagawa, S., Maeda, A., Kawamura, T., Ueno, T., Usui, N., Kondo, S., Matsumoto, S., Okitsu, T., Goto, M., and **Nagashima, H.**	A comparison of the main structures of N-glycans of porcine islets with those from humans	Glycobiology	vol. 24	25–38	2014
Nishimura, S., Nagasaki, M., Okudaira, S., Aoki, J., Ohmori, T., Ohkawa, R., Nakamura, K., Igarashi, K., Yamashita, H., Eto, K., Uno, K., Hayashi, N., Kadowaki, T., Komuro, I., Yatomi, Y., and Nagai, R.	ENPP2 contributes to adipose Tissue expansion and insulin resistance in diet-induced obesity	Diabetes	vol. 63, no. 12	4154–4164	2014
Tanaka, M., Ikeda, K., Suganami, T., Komiya, C., Ochi, K., Shirakawa, I., Hamaguchi, M., **Nishimura, S.**, Manabe, I., Matsuda, T., Kimura, K., Inoue, H., Inagaki, Y., Aoe, S., Yamasaki, S., and Ogawa, Y.	Macrophage-inducible C-type lectin underlies obesity-induced adipose tissue fibrosis	Nature Communica-tions	vol. 5	4982	2014

研究成果の刊行物・別刷

Cell Stem Cell
Clinical Progress

Expandable Megakaryocyte Cell Lines Enable Clinically Applicable Generation of Platelets from Human Induced Pluripotent Stem Cells

Sou Nakamura,[1] Naoya Takayama,[1] Shinji Hirata,[1] Hideya Seo,[1] Hiroshi Endo,[1] Kiyosumi Ochi,[1] Ken-ichi Fujita,[1] Tomo Koike,[1] Ken-ichi Harimoto,[1] Takeaki Dohda,[1] Akira Watanabe,[2] Keisuke Okita,[2] Nobuyasu Takahashi,[3] Akira Sawaguchi,[3] Shinya Yamanaka,[2] Hiromitsu Nakauchi,[4] Satoshi Nishimura,[5,6] and Koji Eto[1,4,*]
[1]Department of Clinical Application, Center for iPS Cell Research and Application (CiRA), Kyoto University, 606-8507, Japan
[2]Department of Reprogramming Science, CiRA, Kyoto University, 606-8507, Japan
[3]Department of Anatomy, Ultrastructural Cell Biology, Faculty of Medicine, University of Miyazaki, Miyazaki 889-1692, Japan
[4]Laboratory of Stem Cell Therapy, Center for Stem Cell Biology and Regenerative Medicine, Institute of Medical Science, The University of Tokyo, Tokyo 108-8639, Japan
[5]Department of Cardiovascular Medicine, The University of Tokyo, Tokyo 113-8655, Japan
[6]Department of Cell and Molecular Medicine, Center for Molecular Medicine, Jichi Medical University, Tochigi 329-0498, Japan
*Correspondence: kojieto@cira.kyoto-u.ac.jp
http://dx.doi.org/10.1016/j.stem.2014.01.011

SUMMARY

The donor-dependent supply of platelets is frequently insufficient to meet transfusion needs. To address this issue, we developed a clinically applicable strategy for the derivation of functional platelets from human pluripotent stem cells (PSCs). This approach involves the establishment of stable immortalized megakaryocyte progenitor cell lines (imMKCLs) from PSC-derived hematopoietic progenitors through the overexpression of BMI1 and BCL-XL to respectively suppress senescence and apoptosis and the constrained overexpression of c-MYC to promote proliferation. The resulting imMKCLs can be expanded in culture over extended periods (4–5 months), even after cryopreservation. Halting the overexpression of c-MYC, BMI1, and BCL-XL in growing imMKCLs led to the production of CD42b$^+$ platelets with functionality comparable to that of native platelets on the basis of a range of assays in vitro and in vivo. The combination of robust expansion capacity and efficient platelet production means that appropriately selected imMKCL clones represent a potentially inexhaustible source of hPSC-derived platelets for clinical application.

INTRODUCTION

Platelets generated from megakaryocyte (MK) precursors are vital for the treatment of many hematological diseases and traumas. Currently, platelets can only be obtained through blood donation. Fresh single-donor platelets have a short shelf life and must be maintained with plasma at 20°C–24°C; they readily lose clotting activity when pooled from multiple donors and frozen or warmed to 37°C (Bergmeier et al., 2003; Nishikii et al., 2008). Moreover, repeated transfusion induces the production of antibodies against allogenic human leukocyte antigen (HLA) or human platelet antigen (HPA) on the transfused platelets (Schiffer, 2001), which renders the patient unresponsive to platelet transfusion therapy. These supply logistics and practical limitations represent barriers to the widespread application of platelets as a resource for patients. In that context, human induced pluripotent stem cells (hiPSCs) (Takahashi et al., 2007) could represent a potent alternative source of platelet production. Because platelets do not contain nuclei, gamma irradiation before transfusion could be used to eliminate any residual contaminating hiPSCs and their derivatives, reducing the risk of tumorigenesis. Thus, the application of iPSC-based technology could potentially yield a consistent supply of HLA- and/or HPA-matched or even autologous platelets in a way that would address some of the major roadblocks in the current clinical approaches to platelet-based therapy.

Our group and another recently demonstrated that hiPSCs derived from human skin fibroblasts or blood cells or from human embryonic stem cells (hESCs) can be used to generate platelets in vitro and that these platelets appeared to function normally when transfused into mouse models (Takayama et al., 2010; Lu et al., 2011). However, the yield of platelets was still far below what would be required to generate even 1 u of platelet concentrate for patient transfusion. Recent studies have shown that self-replicating MK progenitors can be directly generated from murine hematopoietic stem cells (HSCs) within bone marrow (BM) in vivo (Yamamoto et al., 2013), but there was no evident way to sustain long-term self-replication of MK progenitors in vitro. We previously showed that the activation of c-MYC to a restricted level below that associated with senescence and apoptosis induction appears to lead to an increase in platelet generation (Takayama et al., 2010). In the present study, we show that co-overexpression of c-MYC and BMI1, a polycomb complex component that represses the *INK4A/ARF* gene locus (Oguro et al., 2006), enables megakaryocytic cell lines (MKCLs) derived from hiPSCs or hESCs to grow continuously for up to 2 months. A destabilization domain (DD) vector system (Banaszynski et al., 2006) enabled us to control exogenous c-MYC within the appropriate range, leading to successful induction of

Cell Stem Cell *14*, 535–548, April 3, 2014 ©2014 Elsevier Inc.

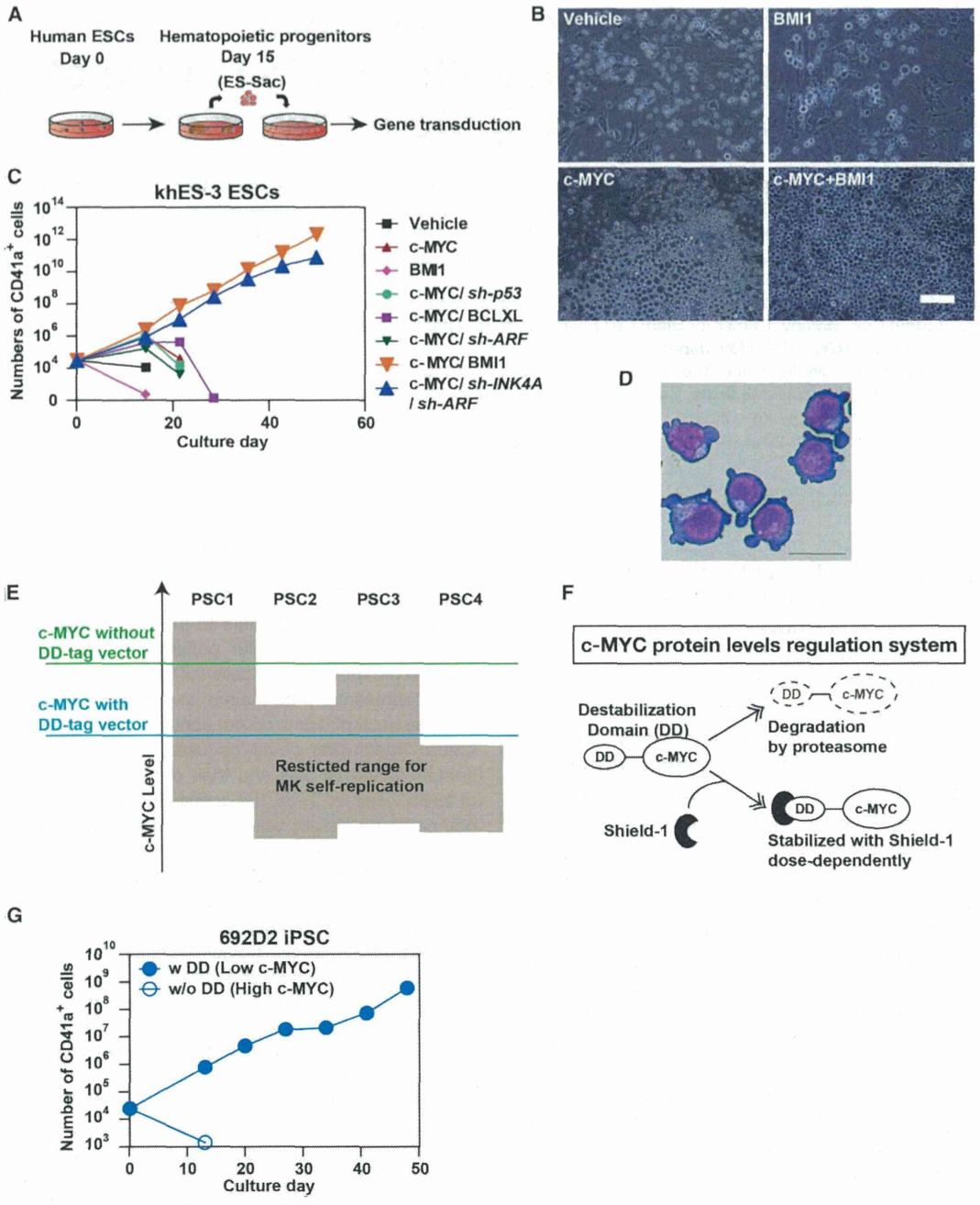

Figure 1. Induction of a Megakaryocyte Progenitor Cell Line from Human Embryonic Stem Cells and Induced Pluripotent Stem Cells Was Induced by Restricted Range of c-MYC Overexpression along with BMI1 Overexpression

(A) Scheme for inducing megakaryocyte progenitor cell lines (MKCLs) from human PSCs. The targets for gene transduction are hematopoietic progenitors, including the $CD34^+$ population.

(B) Representative photomicrograph of cells transduced with vector alone, c-MYC alone, BMI1 alone, or a combination of c-MYC and BMI1 (200×). The scale bar represents 100 μm.

(C) Numbers of $CD41a^+$ cells after gene manipulation. Hematopoietic progenitor cells (HPCs) within human embryonic stem cell (hESC; KhES-3 clone) sacs were collected and transduced with noninducible retroviral vectors with vector alone (GFP alone), c-MYC alone, BMI1 alone, or combinations of c-MYC plus *p53* knockdown, c-MYC plus *ARF* knockdown, c-MYC plus BCL-XL, c-MYC plus *INK4A/ARF* knockdown (blue), or c-MYC plus BMI1 (orange). The combinations of c-MYC plus BMI1 and c-MYC plus *INK4A/ARF* knockdown induced exponential growth in $CD41a^+$ megakaryocytes (MKs). Results are expressed as means from two to three independent experiments.

(D) Representative image of May-Giemsa-stained MKCLs. The scale bar represents 20 μm.

(legend continued on next page)

MKCLs. The addition of BCL-XL made it possible to obtain immortalized MKCLs (imMKCLs) that can be grown for more than 5 months and thus function as candidate cell banks. When the expression of c-MYC, BMI1, and BCL-XL is turned off, imMKCLs produce functional CD42b (glycoprotein Ib α [GPIbα] and receptor for von Willebrand factor [vWF])$^+$ platelet particles. The expression of CD42b on platelets is required for the initiation of clotting (Ware et al., 2000) and bacterial clearance in vivo (Wong et al., 2013). Although previous studies have reported that CMK, Meg01, and K562 cells, three well-known MK lineage leukemia cell lines, can become polyploid and release CD41a$^+$ particles in the presence of agonist stimulation, they do not provide a suitable source for a platelet supply because the particles are CD42b$^-$ (Isakari et al., 2009; Sato et al., 1989; Terui et al., 1998). In this report, we describe a strategy that involves MKCLs with long-term self-renewal capacity and the potential to provide an inexhaustible supply of CD42b$^+$ platelets; in that respect, they resemble endogenous self-replicating MK progenitors identified in vivo (Yamamoto et al., 2013). Clinical application of this technology could provide a plentiful supply of platelets from suitably screened and selected imMKCL clones to serve as cell bank stocks with minimal risk of adverse side effects.

RESULTS

Induction of Expandable MK Progenitor Cells from Human PSCs with c-MYC and BMI1

We previously showed that, when expressed at an appropriate level, c-MYC acts as a growth mediator in normal megakaryopoiesis and thrombopoiesis from hESCs or hiPSCs, whereas excessive c-MYC expression in hematopoietic progenitor cells (HPCs) induces the activation of the INK4A and ARF pathways, leading to senescence and apoptosis (Takayama et al., 2010). Therefore, we hypothesized that c-MYC activation might contribute to self-replication at the MK progenitor stage. When we assessed the effects of c-MYC overexpression alone, BMI1 overexpression alone, c-MYC overexpression plus *p53* knockdown, c-MYC plus BCL-XL overexpression, and c-MYC plus BMI1 overexpression in CD34$^+$CD43$^+$-containing HPCs derived from the KhES-3 hESC line, we found that c-MYC overexpression alone or the combination of c-MYC and BMI1 overexpression increased numbers of large cells expressing megakaryocytic CD41a$^+$CD42a (GPIX)$^+$CD42b$^+$CD9$^+$ markers over a 2-week period (Figures 1A–1C; Figure S1A available online). With c-MYC and BMI1 overexpression (Figure 1C, orange triangles) or c-MYC overexpression and *INK4A/ARF* knockdown (Figure 1C, blue triangles), but none of the other aforementioned conditions, proliferation of this cell population was maintained at an exponential level for 2 months (MK progenitor cell line; Figure 1C, orange triangles) and was dependent upon the presence of thrombopoietin (TPO) with the help of stem cell factor (SCF). This suggests that the effect of BMI1 may be to at least inhibit INK4A/ARF-dependent senescence and apoptosis during the initiation of self-replication, as confirmed by quantitative PCR (qPCR) analysis, which revealed BMI1 represses c-MYC-induced the upregulation of *INK4A/ARF* (Figure S1B). The CD41a$^+$ MKCLs derived from hESCs showed monoblastic morphology with basophilic cytoplasm (Figure 1D) and generated aberrant platelet-like particles expressing normal levels of CD41a but reduced levels of CD42b (Figure S1C). This is consistent with the requirement for the downregulation of c-MYC for maturation of MKs (Takayama et al., 2010).

A Defined c-MYC Expression Level Is Important for MKCL Induction and Robust Expansion

Our ability to induce MKCLs with c-MYC and BMI1 overexpression and then grow the cells for more than 2 weeks varied among individual PSC clones (data not shown). Therefore, we suspected that individual PSC clones require different levels of c-MYC. When we prepared an inducible all-in-one vector harboring c-MYC and BMI1 (Ohmine et al., 2001) (Figure S1D), we obtained clearer evidence that c-MYC levels are crucial for the sustained growth of MKCL, given that we saw different results with c-MYC-2A-BMI1 and BMI1-2A-c-MYC gene sequences in this vector (Figures S1E and S1F). Furthermore, to confirm the hypothesis that, in some individual PSC clones, the effective c-MYC expression level may be restricted to a specific range (Figure 1E), we used a vector tagged with a DD (Banaszynski et al., 2006) in order to reduce the level of c-MYC protein (Figure 1F). This system regulates protein stability, and thus the level of c-MYC expression, in a manner that depends on the Shield1 concentration (NIH 3T3 cells in Figure S1G). When we used this DD-tagged vector system to establish iPSC (692D2)-derived MKCLs, we found that 692D2 iPSCs showed no self-replication when transduced with c-MYC-2A-BMI1 overexpression without a DD tag, but transduction of the DD tag vector without the addition of Shield1 allowed clone 692D2 to grow for up to 50 days in culture (Figure 1G). This self-replication was inhibited by 100 or 1,000 nM Shield1 (Figure 2Ai), suggesting the total c-MYC level most likely blocked stable self-replication. This result was not due to nonspecific cell toxicity (Figure S2A) or activation of the *INK4A/ARF* gene locus by the high level of c-MYC, given that levels of *p14* and *p16* mRNA (derived *INK4A/ARF* locus gene) did not differ in the presence or absence of 1,000 nM Shield1 (Figure S2B).

Given that BMI1, which is also overexpressed in our system, represses the *INK4A/ARF* gene locus, the mechanism underlying the MYC-dependent failure of continuous self-replication was unclear. However, the well-known involvement of c-MYC in caspase-dependent apoptosis (Juin et al., 2002) prompted us to assess caspase activity in the MKCL clone. Caspase assays revealed that the activation of caspases 3 and 7 in DD

(E) Schematic diagram illustrating the hypothesis that there is an association between c-MYC levels and MK self-replication. Individual human PSC clones (hESCs or hiPSCs) define the c-MYC activation window (restricted range) needed to induce MK self-replication.
(F) Scheme for a c-MYC regulation system using a destabilization domain (DD). Proteins with a DD are rapidly destroyed via the ubiquitin-proteasome pathway. Administration of Shield1 putatively inhibits DD-mediated degradation in a concentration-dependent manner.
(G) Numbers of CD41a$^+$ MKs determined by flow cytometry. MKs were derived from iPSCs (692D2) transduced with inducible c-MYC-DD-2A-BMI1 (with [w] DD) or inducible c-MYC-2A-BMI1 retroviral vector (without [w/o] DD; see Figure S2A).

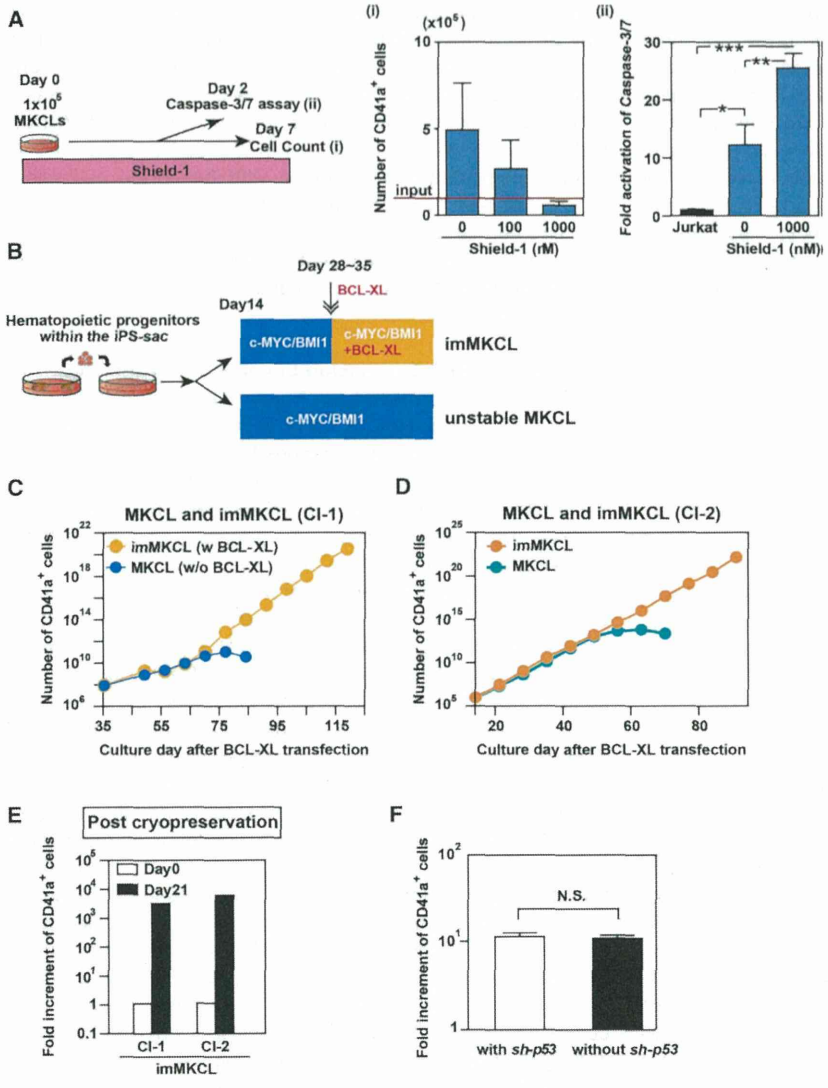

Figure 2. Later Expression of BCL-XL Inhibited Caspase Activation Induced by Excessive c-MYC, Stabilizing Cell Growth and Contributing to the Establishment of imMKCLs

(A) Relationship between the c-MYC expression level, cell viability, and caspase activity. (i) Numbers of live CD41a$^+$ MKs derived from hiPSC (692D2)-based MKCLs generated with an inducible DD vector in the absence or presence of the indicated concentrations of Shield1. (ii) Caspase 3 and 7 activity in samples of Jurkat cells (control, fold = 1, black bar) or hiPSC (692D2)-derived MKCLs on day 2 of culture after transduction with a DD system in the absence or presence of 1,000 nM Shield1. *$p < 0.05$; **$p < 0.01$; ***$p < 0.001$. Results are expressed as means ± SE from five independent experiments.

(B) Scheme for generating unstable MKCLs with c-MYC and BMI1 (2F) or imMKCLs with c-MYC, BMI1, and BCL-XL (3F).

(C and D) Additional transduction of *BCL-XL* gene improved the growth curve for CD41a$^+$ MKs derived from hiPSC (692D2)-derived MKCLs with a DD system (C; clone 1 [Cl-1]) and from hESCs (KhES3)-derived MKCLs (D; Cl-2). Yellow circles indicate the numbers of cells obtained with 3F, and blue circles indicate 2F. Cell numbers were calculated cumulative values.

(E) Increment in CD41a$^+$ cells derived from Cl-1 and Cl-2 after cryopreservation. Results were an average of two independent experiments.

(F) The additional effect of *p53* knockdown on immortalization of MKCLs. Results are expressed as means ± SE from three independent experiments.

self-replicable MKCLs derived from iPSC clone 692D2 was 2-fold higher in the presence of 1,000 nM Shield1 than in its absence. This increased caspase activation was also associated with reduced cell viability (Figures 2Ai and 2Aii), confirming that restricting caspase activation may be key to successfully establishing expandable MKCLs (Figure S2B). Notably, caspase activation in the absence of Shield1 was still 12.2× higher than in Jurkat cells (Figure 2Aii). Some apoptotic events are transcriptionally determined (Chen et al., 2007; Kumar and Cakouros, 2004). Therefore, to further address the mechanism by which excessive c-MYC represses self-replication and induces apoptosis, we carried out a microarray analysis with iPSC-derived MKCLs treated with or without 1,000 nM Shield1. Gene ontology classification of genes differentially expressed in the presence and absence of Shield1 indicated a correlation between higher levels of c-MYC (1,000 nM Shield1) and the expression of the proapoptotic factors *BMF* and *BBC3* (*PUMA*), which can contribute to the release of cytochrome-c from mitochondria via mitochondrial outer membrane permeabilization. High levels of c-MYC also influenced cell-cycle-related genes, increasing the expression of cyclin-dependent kinase inhibitors (*CDKN1B*, *p27*, and *Kip1*), which could arrest MKCL growth. These changes were also confirmed by qPCR analysis (Figures S2C and S2D). Thus, high c-MYC expression can lead to caspase-dependent MKCL apoptosis (Figure 2A), despite the suppression of the INK4A/ARF pathway by BMI1 (Figure S2B). These data again indicate that alternative apoptosis pathways, as well as the INK4A/ARF pathways, are independently induced by excessive c-MYC in individual PSC-derived MKCL clones.

Suppression of Caspase Activation through BCL-XL Expression Promotes Immortalization

We noticed that MKCLs obtained from either ESC clone KhES3 or iPSC clone 692D2 with c-MYC plus BMI1 (Figure 2B, bottom line) exhibited limited growth potential and discontinuous cell growth that ceased at about 60 days, potentially reflecting an increase in caspase activation (692D2 cell growth in Figure 2C; KhES3 cell growth in Figure 2D; 0 nM Shield1for 692D2 in Figure 2Ai and KhES-3 in Figure S2E). Thus, it appears that the expression of c-MYC and BMI1 alone are not suitable for

generation of an immortalized cell line. We therefore sought to examine the effect of BCL-XL on days 14–21 after transduction of c-MYC plus BMI1 (Figure 2B). We found that BCL-XL overexpression induced exponential growth of $CD41a^+$ cells derived from either 692D2 or KhES3 cells. This growth persisted for over 5 months, and we therefore deemed these cells to be self-renewing imMKCLs (Figures 2C and 2D for 692D2 [imMKCL clone 1, Cl-1], and Figure 2D for KhES-3 ESCs [Cl-2]; yellow circles). These two imMKCLs also showed comparable growth after cryopreservation (Figure 2E) as well as somewhat larger cell size and expression of CD41a, CD42a, CD42b, and CD9 (Figure S2F). Growth of these imMKCLs was sustained even with higher c-MYC expression in the presence of 100 or 1,000 nM Shield1 (Figures S2G–S2I), and the cells exhibited comparatively low levels of caspase 3 and 7 activation, similar to that of Jurkat cells (Figure S2I).

To further validate the function of BCL-XL in caspase regulation, we tested the effect of the caspase inhibitor Z-VAD FMK on proliferation. Caspase inhibition increased proliferation about 21-fold, whereas BCL-XL expression elicited a 64-fold increase. In contrast, the vehicle control (DMSO) enhanced apoptosis (Figures S3A–S3C). Altogether, these findings again confirm that BCL-XL inhibits apoptosis through caspase 3 and 7 inactivation and that c-MYC, BMI1, and BCL-XL are all required for the induction of imMKCLs from PSC clones. In addition, because it is well known that activation of p53 and p21 is also associated with c-MYC-dependent apoptosis (Hotti et al., 2000), we assessed the effect of inhibiting p53 on cell growth with imMKCL Cl-1. Our results show no involvement of p53 in cells expressing c-MYC, BMI1, and BCL-XL (Figure 2F), and a similar result was obtained with KhES-3-imMKCL (Cl-2; data not shown).

Next, we asked whether the simultaneous overexpression of c-MYC, BMI1, and BCL-XL was more suitable for establishing imMKCLs than overexpression of c-MYC plus BMI1 followed by later expression of BCL-XL. To address that question, we used four individual PSC clones to compare two protocols: simultaneous overexpression of all three genes or overexpression of c-MYC and BMI1 followed by BCL-XL 14–21 days later, counting from the HPC stage (days 28–35 from the hESC or iPSC stage; Figure 2B, top). Simultaneous addition of all three genes promoted maximal proliferation for only up to 40–50 days, whereas stepwise addition of c-MYC and BMI1 followed by BCL-XL consistently showed more sustained proliferation with all clones examined (Figure S3D–S3G).

One potential caveat to this approach is that long-term cultivation might lead to imMKCLs becoming oncogenic. Interestingly, after cultivation for 5 months, two of three imMKCLs, Cl-1 and Cl-2 but not Cl-7, consistently showed a specific karyotypic abnormality: chromosomal translocation that included chromosome +1 or −5 (Figure S4A). When these two clones were separately infused into immunodeficient mice, one (n = 5) displayed leukemogenesis contributing to early death, but the other did not (Figure S4B). These results highlight the importance of transplantation studies with imMKCLs for clone selection. Interestingly, Cl-7 exhibited no karyotypic abnormality (Figure S4A) and consistently showed no abnormalities in transplantation studies (up to 16 weeks; Figure S4B). Therefore, we suggest that combined analysis, including both karyotypic examination and transplantation of individual imMKCL clones, would be useful for selecting imMKCLs as cell bank stock candidates.

Differentiation Phase of imMKCLs for Upregulation of CD42b during Maturation

The GPIb-V-IX complex, particularly CD42b (GPIbα), on platelets is a key binding site for vWF and is required for the initial adhesion of platelets to an injured vessel wall (Ware et al., 2000) as well as normal circulation after transfusion (Leytin et al., 2004). Platelets lacking CD42b expression are quickly cleared from the circulation in vivo, leading to insufficient numbers of circulating platelets after transfusion (Nishikii et al., 2008). Assuming that the downregulation of c-MYC would be required for the generation of $CD42b^+$ platelets (Takayama et al., 2010), we turned off the expression of all three inducers (c-MYC, BMI1, and BCL-XL). Five days after these genes were turned off under serum-free conditions (Figure 3A), the iPSC-derived imMKCLs had changed to exhibit MK polyploidization (Figure 3B; on, 5.5% [left]; off, 20.2% [right]) as well as proplatelet formation (Figure 3C and Movie S1) with increased CD42b expression. This is exemplified by the two imMKCL clones in Figure 3D. Along with those changes, after turning off the expression of the exogenous inducing genes, both endogenous and exogenous *c-MYC*, *BMI1*, and *BCL-XL* expression declined (Figure S5A), and transcription factors associated with MK maturation, *GATA1*, *FOG1*, *NFE2*, and *β1-tubulin* increased to levels comparable to or higher than those seen in cord blood (CB)-derived MKs (Figure 3E).

Induction of Efficient Yield of $CD41a^+CD42b^+$ Platelets

Turning *c-MYC*, *BMI1*, and *BCL-XL* off with a doxycycline-regulated system increased the $CD42b^+$ platelet yield from imMKCLs and upregulated CD42b expression in $CD41a^+$ platelets (Figures 4A and 4B), in comparison to maintaining the overexpression of the three factors or *BCL-XL* alone (Figure S5B). In addition, whereas imMKCLs generated significant numbers of $CD41a^+$ $CD42b^+$ particles that closely resembled endogenous platelets, the well-known MKCLs Meg01, CMK, and K562, produced mostly $CD41a^+$, but $CD42b^-$, platelet-like particles (Figure S5C). We estimated production to be three $CD42b^+$ platelets per Cl-2 imMKCL-MK and 10 platelets per Cl-7 imMKCL-MK after the induction of differentiation (5 days after exogenous expression was turned off; Figure S5D) under serum-free conditions, which is a suitable level for clinical application. In a 10-cm dish scale (10 ml), 4×10^6 and 2×10^6 platelets per ml were obtained from imMKCL Cl-7 and Cl-2, respectively (Figure 4C). Therefore, our proposed system could theoretically yield 10^{11} platelets (equivalent to one transfusion) within 5 days with 25–50 l medium.

Characterization of platelet yields using flow cytometry revealed that the expression levels of platelet-functional molecules, including CD42b, CD61 (β3 integrin), protease-activated receptor 1 (PAR1; thrombin receptor), CD49b (α2 integrin), and CD29 (β1 integrin), were mostly comparable to those seen in fresh human peripheral blood (PB)-derived platelets and higher than in human endogenous pooled platelets, although the expression of GPVI (GP6) was a little weaker than it was in fresh PB (Figure 4D), possibly because of receptor shedding at 37°C (Gardiner et al., 2012). At the ultrastructural level, transmission

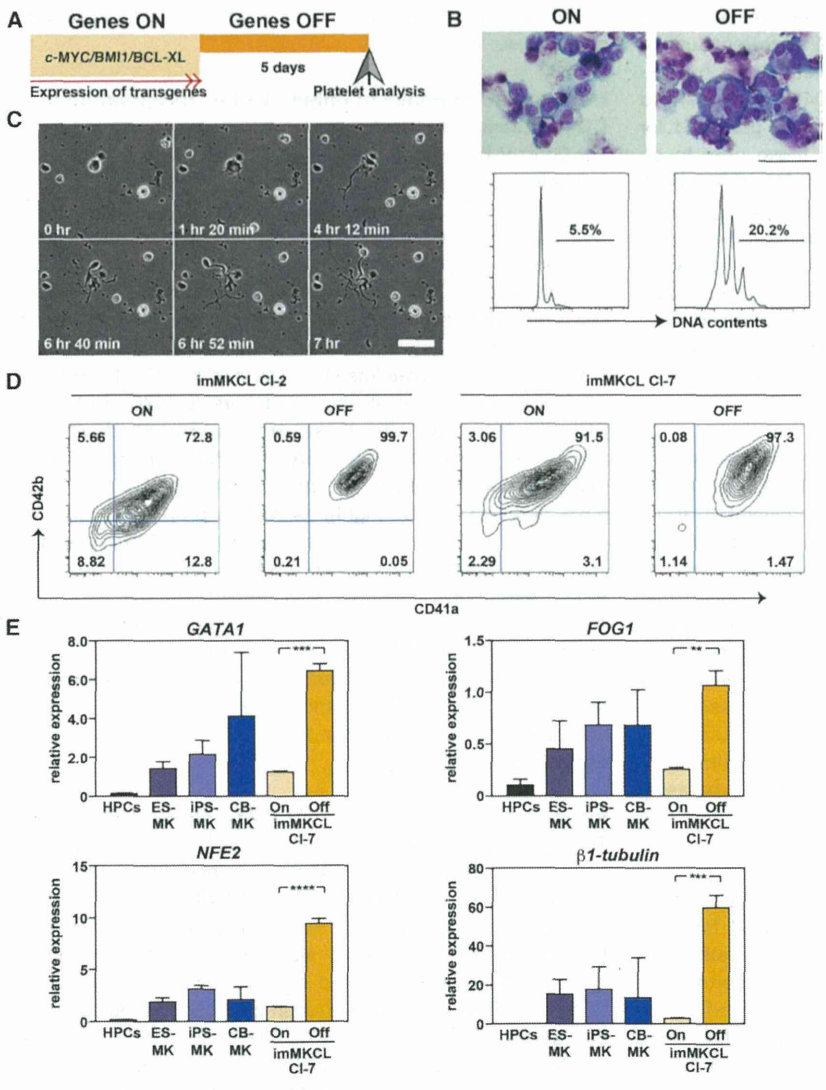

Figure 3. Turning Off 3F Transgenes Promoted the Maturation of MKs from imMKCLs

(A) MKs and platelets were analyzed 5 days after turning off 3F (cMYC, BMI1, and BCL-XL) expression.

(B) Giemsa staining (top pictures) and flow cytometric analysis of ploidy among imMKCLs with and without 3F expression (genes on or genes off). The scale bar represents 50 μm.

(C) imMKCL Cl-7 examined with time-lapse microscopy 4 days after genes were turned off. Sequential images showing proplatelet formation. The scale bar represents 50 μm.

(D) Representative contour plots for imMKCL Cl-2 and Cl-7 (MK populations are shown in side and forward scatter contour plots in a flow cytometer) derived from ESCs and iPSCs (KhES3 and DN-SeV2, respectively).

(E) qPCR analysis of *GATA1*, *p45 NF-E2*, *FOG1*, and *β1-tubulin* gene expression. Samples were obtained from hiPSC-derived $CD34^+/CD43^+/CD41a^-/GPA^-$ HPCs (Sac-HPCs), Sac-dependent MKs from ESCs and iPSCs, MKs derived from cord blood (CB)-$CD34^+$ cells, and imMKCL Cl-7 (DN-SeV2 iPSC clone) in the presence (on) or absence (off) of 3F. Gene expression was normalized to GAPDH expression. 3F was transduced into Sac-HPCs as described in the Experimental Procedures. Results are expressed as means ± SE from three independent experiments.

electron microscopy revealed frequent generation of platelets through cytoplasmic fragmentation (Figure S6A) and proplatelets in the culture dish (Figure 3C and Movie S1). Individual imMKCL-derived platelets showed normal microtubules but fewer granules when compared to fresh human donor platelets (Figure 5A and S6A). To explore the functionality of imMKCL-derived platelets, we used flow cytometry to examine integrin αIIβ3 activation (inside-out signaling) or platelet aggregation after stimulation with platelet agonists (De Cuyper et al., 2013). Agonist stimulation increased PAC-1 binding mean fluorescent intensity, given that this antibody binds to the activated form of αIIbβ3 integrin (Figures 5B and 5C) as well as platelet aggregation (Figure 5D), clot retraction (Figure 5E), actin cytoskeletal changes (Figure S6B), and vWF or ADP secretion (Figure S6C). Collectively, most in vitro functional parameters indicated that imMKCL platelets gave less robust responses than fresh human platelets, but, comparison to pooled human endogenous platelets (Figures 5C and 5D) or iPSC-derived platelets generated with a direct differentiation method (data not shown; Takayama et al., 2010) indicated their functionality was still sufficient to be useful. We also used an ex vivo flow chamber system within which human vWF (10 μg/ml) was immobilized and a shear rate of 1,600 s^{-1} was applied. imMKCL platelets showed 62.3% (Cl-2) and 75.8% (Cl-7) of the CD42b-dependent binding of fresh human platelets, and human CD42b blocking antibody reversed this adhesion (Figure 5F). With our current protocol, final platelet collection takes place during the final 5 days in the absence of serum at 37°C. Altogether, these two conditions may account for the relatively low granule content (Figure S6C) and diminished aggregation (Figure 5D).

imMKCL-Derived Platelets Show Thrombogenic Activity in Mouse Models of Thrombocytopenia

Next, we evaluated the in vivo circulation of imMKCL platelets with previously optimized transfusion models (Takayama et al., 2010). Using NOD/SCID/IL-2Rg-null (NOG) mice with irradiation-induced thrombocytopenia, flow cytometric analyses were carried out 30 min, 2 hr, and 24 hr after transfusion (1 or 6 × 10^8 platelets per mouse). The posttransfusion kinetics of imMKCL-derived platelets were nearly the same as those obtained with fresh human platelets (n = 4 individual groups in two independent experiments; Figures 6A and 6B). To further assess the functionality of imMKCL platelets in vivo, we used

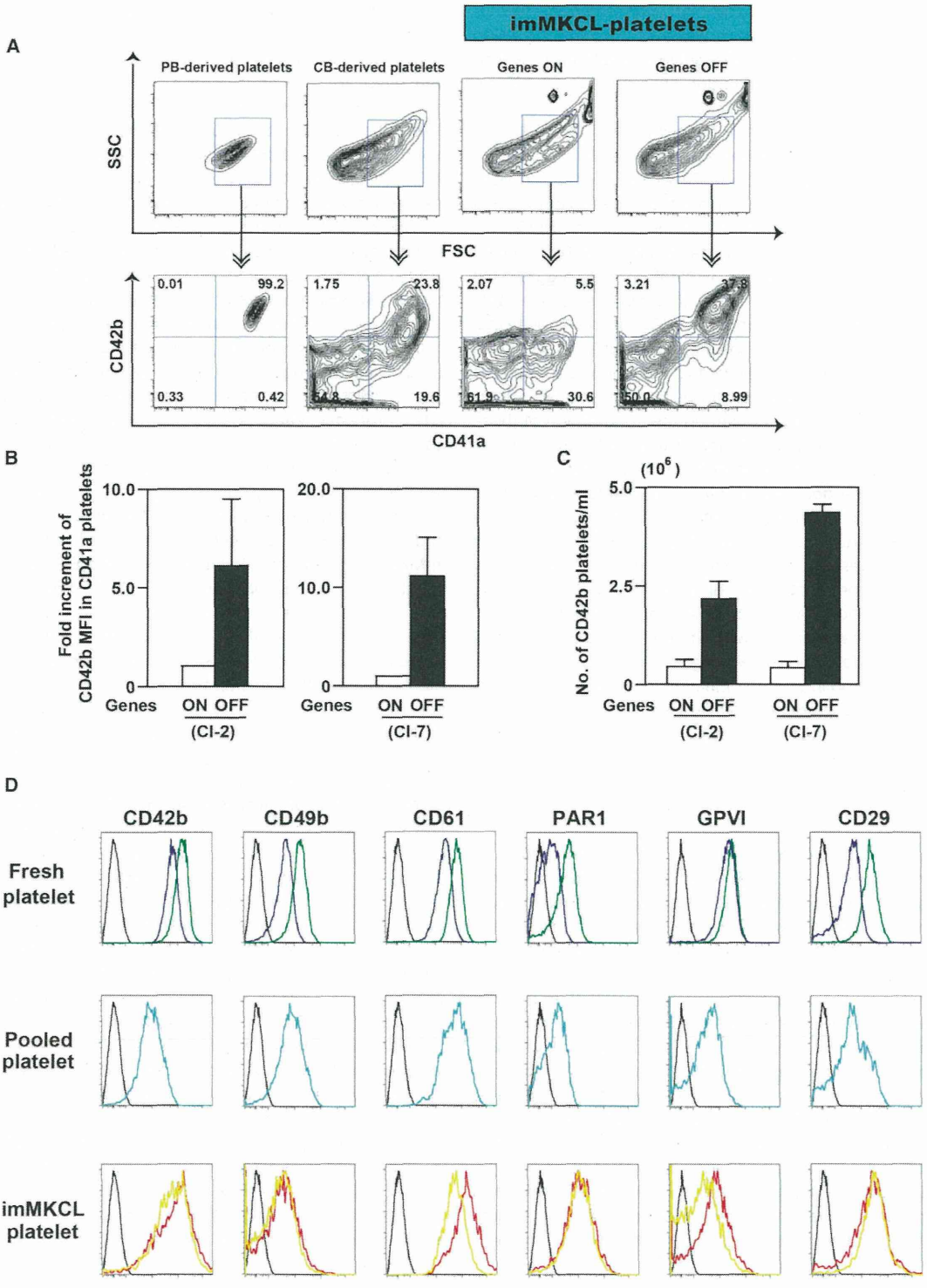

Figure 4. imMKCL-Derived Mature MKs Generated CD41a$^+$CD42b$^+$ Platelets upon Turning Off 3F Transgenes

(A) Representative contour plots for human peripheral blood (PB)-, CB-CD34$^+$HS/PC-, and imMKCL (3F on and off)-derived platelets (platelet population are shown in side and forward scatter contour plots).

(B) Fold increment in CD42b$^+$ mean fluorescent intensity (MFI) among CD41a$^+$ imMKCL CI-2 (KhES3)- and CI-7 (DN-SeV2)-derived platelets. White bars, genes on; black bars, genes off. Results are expressed as means± SE from three independent experiments. The mean value of the samples with genes on is assigned as 1.0.

(legend continued on next page)

thrombocytopenic NOG mice and high-spatiotemporal-resolution confocal laser microscopy to visualize the initial adhesion of individual platelets to laser-exposed vessel walls and the subsequent thrombus formation under flow conditions without apparent endothelial disruption (Takizawa et al., 2010; Nishimura et al., 2012). Using fresh human platelets or imMKCL-derived platelets labeled with carboxyfluorescein diacetate and succinimidyl ester, along with injection of Texas Red dextran to visualize blood cell kinetics, we calculated the numbers of platelets adhering to the endothelium after laser injury in the NOG system (Movie S2). We confirmed that single imMKCL-derived platelets adhere to the vessel without forming aggregates with host platelets. AK4 antibody (antihuman P-selectin) partly reversed the platelet adhesion (i.e., >60% for Cl-2 platelets; Figure 6C), indicating that P-selectin contributed to the initial adhesion of the imMKCL platelets and that endothelial-derived vWF and P-selectin are relevant in our mouse models (Nishimura et al., 2012). We also confirmed the contribution of these platelets to thrombi in vivo. We found that platelets from four different imMKCL clones differentially contributed to the developing thrombi to a degree that was at a minimum better than human endogenous pooled platelets ($n = 40$ vessels from three to five animals individually, $p < 0.0001$; Figures 6D and 6E and Movie S3), suggesting that transfer to in vivo conditions may further improve the functionality of imMKCL platelets, perhaps through rejuvenation via endocytosis of granules. Accordingly, our results suggest that, although imMKCL platelets display a smaller capacity for adhesion and aggregation than fresh donor platelets in vitro and in vivo, the functional capacity observed is at a useful level and could potentially be improved by further optimization of the culture conditions and/or the collection method.

DISCUSSION

For successful clinical application of hiPSC technology to platelet transfusion, it will be necessary to produce very large quantities of platelets. To achieve this goal, we will need to boost production efficiency at two stages: the transition from HSCs or myeloid lineage HPCs to MKs and the transition from MKs to platelets (Fuentes et al., 2010; Lu et al., 2011; Takayama et al., 2010; Lambert et al., 2013; Yamamoto et al., 2013). In the present report, we focused on a strategy of generating self-renewing immortalized MKs (Yamamoto et al., 2013), and we have succeeded in establishing imMKCLs with in vitro long-term expansion capacity from human ESCs or iPSCs with three defined factors (c-MYC, BMI1, and BCL-XL) with a temporally hierarchical overexpression protocol (Figures 2 and S3D–S3G). Sustained expansion of these imMKCLs relied on carefully regulated expression of the inducing genes to balance proliferative and apoptotic signals and optimize consistent proliferation. These self-replicating MKs may be applicable in the clinic as a source for a continuous and virtually inexhaustible supply of platelets.

We also showed that the INK4A/ARF and caspase 3 and 7 pathways are activated at the MK progenitor stage when c-MYC levels are too high. The DD derived from mutant human FKBP12 contributes to instability of the tagged protein, but the effect is attenuated by addition of Shield1 (Banaszynski et al., 2006). By using a DD tag vector system as a tool for investigating the impact of restricted c-MYC levels (Figures 1E–1G and S1G), we confirmed the importance of reducing caspase activity during immortalized self-replication of the MK lineage in the presence of TPO and SCF, which suggests that caspase activity plays a role in the previously observed unstable proliferation of MKs in vitro (Figures 7A–7C). This "constrained protein expression" system could also be useful for studying genes that must be strictly regulated. These findings also suggest the existence of a regulatory pathway distinct from the INK4A/ARF and p53 pathways that exerts a protective effect against oncogenic stress in the MK lineage (Figure 2F).

Exogenous overexpression of *BCL-XL* contributed to long-term self-replication by attenuating caspase 3 and 7 activation, even in the presence of higher c-MYC levels (Figure 7C), and endogenous BCL-XL may be required for the survival of imMKCLs yielding platelets (Figures S5A and S5B). Consistent with that idea, results obtained with BCL-XL-deficient mice indicate that this protein is required for MK survival and platelet release (Josefsson et al., 2011). By contrast, sustained BCL-XL overexpression reportedly has a negative effect on the development of demarcation membranes in MKs and on platelet production (Kaluzhny et al., 2002). However, c-MYC-dependent MK proliferation was also TPO-dependent and required BMI1 to be present prior to BCL-XL (Figures 1C, 2C, 2D, and S3D–S3G). Interestingly, we recently showed that the combination of c-MYC and BCL-XL overexpression in $CD34^+CD43^+$-containing HPCs leads to stable erythroblast self-replication induced by erythropoietin (Hirose et al., 2013) but not MK lineage growth (Figure 1C). Thus, distinct combinations of c-MYC and BCL-XL and c-MYC and BMI1 appear to provide context-dependent expansion capacity for erythroblast or MK lineages, respectively (Hirata et al., 2013; Yamamoto et al., 2013). It has also been reported that BMI1 directly binds to RUNX1 and core binding transcriptional factor β and acts as a regulator during megakaryopoiesis (Yu et al., 2012), suggesting that BMI1 may have an alternative function in imMKCL development. The MK proliferation program may be disrupted when the effects of BCL-XL dominate before the MK proliferation program is fully established.

For clinical application, the quality of expandable imMKCLs must be strictly validated, and they must be cryopreserved as master cell banks (MCBs) matched to the required HLA and HPA type. After thawing, MCB-derived working cells would be expected to grow within an appropriate and sufficient term and

(C) Numbers of $CD41a^+CD42b^+$ platelets generated from imMKCL Cl-2 (KhES3) and Cl-7 (DN-SeV2) in a 1 ml culture volume. White bars, genes on; black bars, genes off. Results are expressed as means ± SE from three independent experiments.
(D) Histograms show CD42b, CD49b, CD61, PAR1, GPVI, and CD29 expression on platelets (fresh and pooled) derived from normal donors (two different donors) and imMKCL Cl-2 and Cl-7. Donor-derived pooled platelets were pooled at 37°C for 5 days. Fresh human platelets were from donors 1 (purple) or 2 (green). Pooled platelets were from donor 1. imMKCL platelets were from Cl-2 (yellow) and Cl-7 (red). Black lines in all panels indicate IgG control. x axes, MFI (log scale); y axes, counts.

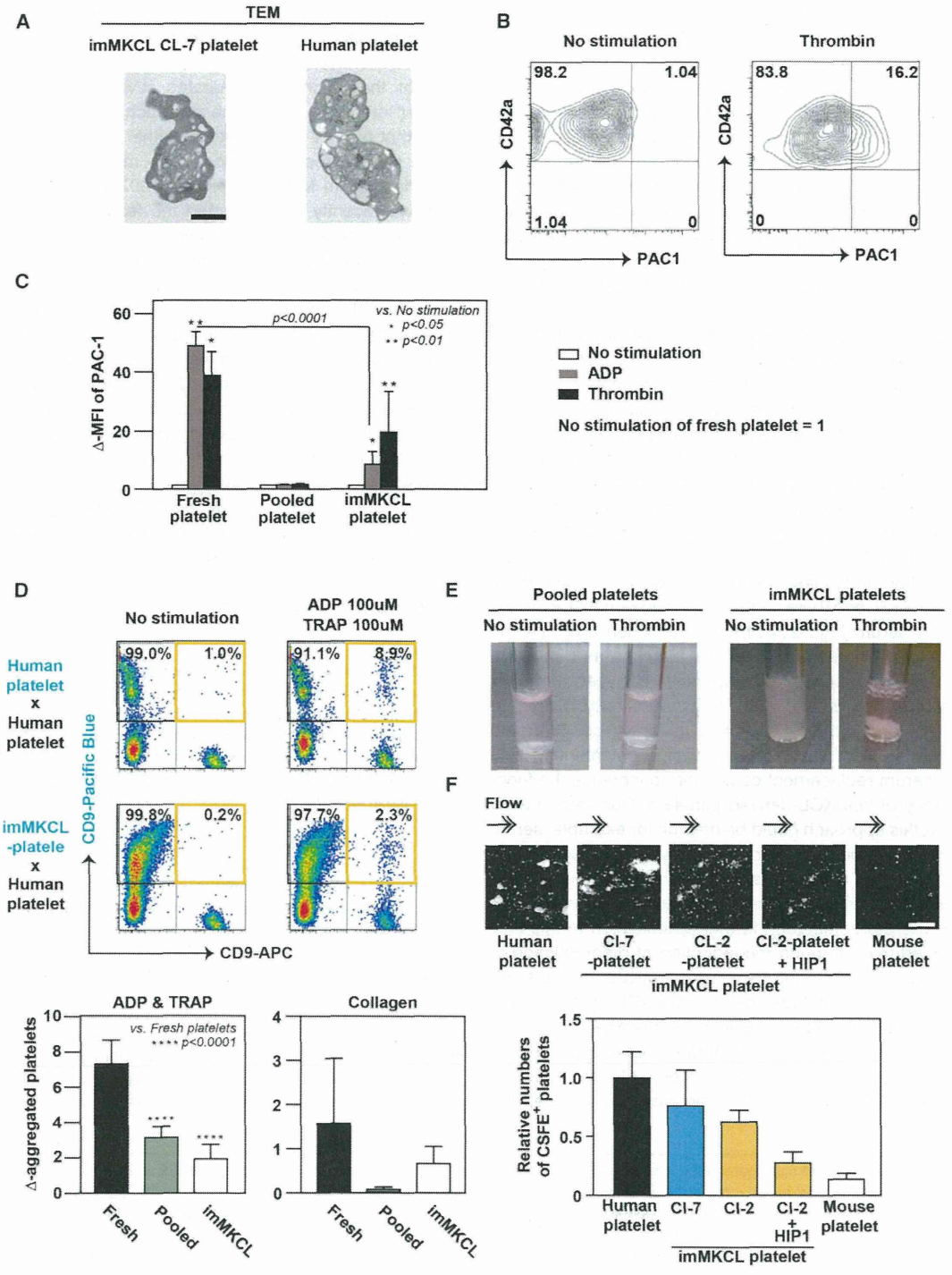

Figure 5. Characterization of imMKCL-Derived Platelets In Vitro

(A) Transmission electron micrographs of an imMKCL Cl-7-derived platelet 5 days after genes off (left) and two fresh donor platelets (right). The imMKCL platelet shows fewer a-granules and dense granules than fresh platelets. The scale bar represents 1 μm.

(B) Representative contour plots for imMKCL platelets showing CD42a (GPIX) and PAC1 bound in the absence or presence of thrombin (1 u/ml).

(C) PAC1 binding to human fresh platelets, human pooled platelets, or imMKCL platelets was quantified by flow cytometry. Data depict means (± SEM) from three independent experiments. y axis indicates ΔMFI calculated as agonist (+) minus no agonist (−). The MFI of agonist (−) was 1.0 in individual samples. ADP (200 μM) or thrombin (1 u/ml) was the agonist.

(legend continued on next page)

generate large numbers of platelets. In this context, continuous culture after cryopreservation (Figure 2E) may enable a continuous supply of platelets through gene manipulation (i.e., a drug-induced genes-off condition). Furthermore, after we had established stably expandable imMKCLs in the presence of serum, we identified two clones that were capable of growing well in liquid culture after adaptation to serum- and feeder-free conditions (Figure S6D). This development suggests that it may well be feasible to use this type of system to generate platelets on the type of industrial scale that can be achieved with tanks.

We compared our current imMKCL/MCB system with our earlier strategy (Takayama et al., 2010). Figure S7 depicts the advantages of the current strategy and its feasibility in terms of three parameters: manipulation, duration, and culture scale. For each parameter in the figure, the top panels show our current protocol, and the bottom panels show the earlier protocol (Takayama et al., 2010). It is important to consider the need to prepare and provide more than 10^{11} platelets, given that 3×10^{11} platelets are required for 1 u of platelet concentrate for transfusion in the United States. We suggest using 10^8 imMKCL cells per vial as a MCB-derived working cell stock, which will produce 2.5×10^{10} MKs in around 14 days (Figures 2C, 2D, and S3D–S3G). In addition, much less medium is required in the current system (Figure S7), and there might be no requirement for mouse feeder cells or serum (Figure S6D). However, when looking at the similarity between human endogenous platelets and imMKCL platelets, there were several discrepancies between the functional parameters in vitro and in vivo (Figures 6C and 6D). In general, platelet concentrate is supplied in highly concentrated serum for transfusion. This suggests that supplementing with serum or a serum replacement could help to increase the functional capacity of imMKCL-derived platelets. Our data already suggest that this approach could be helpful; for example, serum supplementation improved clot retraction with imMKCL-derived platelets (Figure 5E). This is in contrast to endogenous pooled platelets, which did not form clots at all, even with serum supplementation. Therefore, although further optimization of this final step is needed (e.g., through the induction of differentiation at room temperature (20°C –24°C) before imMKCL platelets are clinically useful, we conclude that an imMKCL system could potentially provide useful platelets in large quantities.

As mentioned, another area for further optimization is the platelet yield per MK, the improvement of which would contribute to further reducing the volume. Several earlier reports on in vitro platelet production systems documented similarly limited efficiency of platelet production from single MKs (Ono et al., 2012; Takayama et al., 2008, 2010). In contrast, it is thought that each MK generates several thousand platelets in vivo (Patel et al., 2005). One approach could be to use a bioreactor that mimics the conditions within BM (Patel et al., 2005), where shear stress from blood flow might accelerate platelet biogenesis from MKs (Junt et al., 2007). On the basis of that idea, we recently demonstrated the feasibility of an artificially produced bioreactor with 2D microfluid circulation and biodegradable scaffolds, which increased platelet yield from hESC- and hiPSC-derived MKs (Nakagawa et al., 2013).

In conclusion, the technology outlined in this study sheds light on an exciting avenue for potential iPSC-based platelet supply. This protocol is also being developed for an Investigational New Drug Application to the United States Food and Drug Administration. To achieve that, further optimization of MK maturation and the efficiency of platelet release in a liquid culture system will help to improve the technology as it develops toward clinical application. Ultimately, we believe that, through the integration of a broad range of technologies, it will be feasible through to achieve clinically effective platelet transfusion without a requirement for donor blood.

EXPERIMENTAL PROCEDURES

Ethical Review

KhES-3 hESC clone (Institute for Frontier Medical Science, Kyoto University) was used with approval from the Ministry of Education, Culture, Sports, Science and Technology of Japan. Collection of PB from healthy volunteers was approved by the ethics committee of the Institute of Medical Science at the University of Tokyo and the Kyoto University Committee for Human Sample-Based Experiments. All studies involving the use of human samples were conducted in accordance with the Declaration of Helsinki.

Cells, Reagents, and Mice

KhES-3 hESCs from H. Suemori (Suemori et al., 2006) and human iPSC clones (585A1, 585B1, 606A1, 648B1, 692D2, and DNSeV-2) were used (Okita et al., 2013). Six-week-old NOG mice were purchased from the Central Institute for Experimental Animals. The mice were irradiated at 2.4 Gy in order to induce thrombocytopenia 9 days before transfusion. Then, selected mice (platelets = 5–20 $\times 10^4/\mu l$) were used for studies of posttransfusion platelet kinetics and in vivo imaging of thrombogeneity.

The following vectors were used: pMXs retroviral vector, pGCDNsam retroviral vector, modified pMXs Tet off-inducible retroviral vector (Ohmine et al., 2001), and CSII-based all-in-one inducible lentiviral vector (Ai-LV) (Takayama et al., 2010). Retrovirus production with a 293 Gag, Pol, VSV-G (vesicular stomatitis virus G) system and lentiviral production were as described previously

(D) Flow cytometric detection of aggregated platelets as a double-positive population among human fresh donor platelets stained with CD9-APC or among human fresh donor platelets (top panel in the dot plot) or with imMKCLs platelets (bottom panel in the dot plot) stained with CD9 Pacific Blue after agonist stimulation. In the absence of agonist stimulation, the double-positive population was small. The lower graph contains summarized results showing the percent double-positive platelets (human fresh platelets, pooled platelets, or imMKCL platelets). y axis indicates D-aggregated percentage calculated as agonist (+) minus agonist (–).Results are expressed as means ± SE from seven independent experiments for ADP&TRAP (left) or four independent experiments for collagen (right).

(E) Pictures of clot retraction. Human endogenous pooled or imMKCL (Cl-7) platelets were suspended in 20% platelet-depleted human plasma containing Iscove's modified Dulbecco's medium (1.6×10^8 platelets/ml). Even when supplemented with human plasma, pooled platelets stored without serum showed no clot retraction, whereas imMKCL platelets did.

(F) Ex vivo flow chamber system within which human vWF (10 μg/ml) was immobilized, and the shear rate was 1,600 s^{-1}. Human and mouse PB platelets and imMKCL Cl-2 and Cl-7 platelets were stained with carboxyfluorescein diacetate, succinimidyl ester (CSFE) and analyzed. Top: representative immunofluorescence micrograph of the chamber. Bottom: relative number of $CSFE^+$ platelets adhering to human vWF. HIP-1, human CD42b antibody. The scale bar represents 100 μm. Results are expressed as means ± SE of a total of 20 trials from three independent experiments. The mean value of human platelets is assigned as 1.0.